Effects of Ruxolitinib on fibrosis in preclinical models of systemic sclerosis

Nessrine Bellamri, Marie Lelong, Audrey Joannes, Erwan Le Tallec, Stéphane Jouneau, Laurent Vernhet, Alain Lescoat, Valérie Lecureur

Effects of Ruxolitinib on fibrosis in preclinical models of systemic sclerosis

Nessrine BELLAMRI[1], Marie LELONG[1], Audrey JOANNES[1], Erwan LE TALLEC[1,2], Stéphane JOUNEAU[1,3], Laurent VERNHET[1], Alain LESCOAT[1,2] and Valérie LECUREUR[1*].

1 Univ Rennes, CHU Rennes, INSERM, EHESP, IRSET (Institut de recherche en santé, environnement et travail) –UMR_S 1085, 35000 Rennes, France

2 Department of Internal Medicine, Rennes University Hospital, 35000 Rennes, France

3 Department of respiratory diseases, Competence center for rare pulmonary diseases, Rennes University Hospital, 35000 Rennes, France

[*] *Corresponding author at : Univ Rennes, CHU Rennes, INSERM, EHESP, IRSET (Institut de recherche en santé, environnement et travail) –UMR_S 1085, 35000 Rennes, France*

E-mail address: valerie.lecureur@univ-rennes1.fr

Abstract

Systemic sclerosis (SSc) is an autoimmune fibrotic disorder notably characterized by the production of antinuclear autoantibodies, which have been linked to an excess of apoptotic cells, normally eliminated by a macrophagic efferocytosis. As interferon (IFN) signature and phosphorylation of JAK-STAT proteins are hallmarks of SSc tissues, we tested the hypothesis that a JAK inhibitor, ruxolitinib, targeting the IFN signaling, could improve efferocytosis of IFN-exposed human macrophages *in vitro* as well as skin and lung fibrosis

In vivo, BLM- and HOCl-induced skin thickness and fibrosis is associated with an increase of caspase-3 positive dermal cells and a significant increase of IFN-stimulated genes expression. In BLM-SSc model, ruxolitinib prevented dermal thickness, fibrosis and significantly decreased the number of cleaved caspase-3 cells in the dermis. Ruxolitinib also improved lung architecture and fibrosis although IFN signature was not entirely decreased by ruxolitinib. *In vitro*, ruxolitinib improves efferocytosis capacity of human monocyte-differentiated macrophages exposed to IFN-γ or IFN-β. In human fibroblasts derived from lung (HLF) biopsies isolated from patients with idiopathic pulmonary fibrosis, the reduced mRNA expression of typical TGF-β-activated markers by ruxolitinib was associated with a decrease of the phosphorylation of SMAD2 /3 and STAT3.

Our finding supports the anti-fibrotic properties of ruxolitinib in a systemic SSc mouse model and *in vitro* in human lung fibroblasts.

Keywords: systemic sclerosis, ruxolitinib, lung fibroblast, fibrosis, macrophage, interferon

1. Introduction

Systemic sclerosis (SSc) is a systemic autoimmune disease characterized by endothelial dysfunction, immune over-activation and fibrosis. Interstitial lung disease (ILD) represents the main cause of SSc-related mortality (1). The pathophysiology of SSc remains poorly understood, but it is recognized that genetic and environmental risk factors initiate vascular damages which in turn induce dysregulated immune response (2). This latter is considered as a major contributor of skin fibrosis, also participating in visceral damage including heart and lung involvement (3).

There is increasing evidence for an involvement of macrophages in the pathogenesis of SSc (4), notably attested by tissue–omics analyses which identified an activated macrophage signature (5,6). Macrophages are a heterogeneous population comprising resident macrophages and blood monocytes-derived macrophages that are recruited in inflamed tissues. Inhibition of monocyte recruitment by immunomodulatory drugs such as mycophenolate mofetil was associated with a lower count of skin macrophages and an improvement of skin fibrosis (7). Moreover, a reduction of macrophage activation by nintedanib improved the fibrotic manifestations into the Fra-2 SSc mouse model (8).

Autoantibodies targeting nuclear antigens (antinuclear antibodies, ANA) are detectable in 90-95% of SSc patients (9) and represent key biomarkers for the diagnosis and classification of SSc patients (10). The presence of autoantibodies might be explained by the accumulation and persistence of apoptotic bodies that would not efficiently cleared by phagocytic cells such as macrophages, providing some antigenic materials composed of nucleic acids and nucleoproteins (4,11). Such a defect of efferocytosis was observed in the monocyte-derived macrophages of SSc patients (12) and an accumulation of apoptotic cells was found in the skin biopsies of SSc patient (13). However, the association between impaired efferocytosis and apoptotic cell accumulation has not been explored in SSc to date.

"Self" DNA and the clearance of immune complexes, composed by autoantibodies bound to uncleared cellular debris, might favor the production of interferon (IFN), thereby contributing to the IFN signature detected in blood, PBMCs and skin biopsies from SSc patients (14–16). This IFN signature was associated with the presence of anti-topoisomerase or anti-U1-RNP antibodies (17,18), the worsening of musculoskeletal symptoms and skin involvement (19). Moreover, a large microarray-type study performed on lung tissues of SSc-ILD patients demonstrated that the increased expression of IFN-stimulated genes (ISGs) was associated with ILD-progression (20). Although the importance of IFN signature in SSc pathogenesis is well recognized, its link with the defect of efferocytosis remains to be confirmed.

IFNs exert their immune functions by binding with IFN receptors IFNAR1 and IFNAR2 which dimerize, interacting with the elements of the Janus Kinase (JAK) protein family tyrosine kinase 2 (Tyk2)/ JAK1 and JAK1, respectively. These latter phosphorylate STAT1, STAT2 and IRF9 to form the ISGF3 complex which in turn initiates the transcription of ISGs (21). Several drugs have been designed to target IFN signaling pathway (22). These treatments include monoclonal antibodies targeting IFNARs (23) and small molecule inhibitors like the family of JAK inhibitors (JAKi) (21,24). JAKi such as tofacitinib or ruxolitinib are FDA-approved drugs for autoimmune or inflammatory disorders including rheumatoid arthritis or for graft-versus-host disease, that share many features with SSc. JAKi represent promising treatments as JAK/STAT pathway is activated in both skin and lung of patients with SSc (25). Ruxolitinib, considered as a pan-JAKi, has anti-inflammatory effects by decreasing the expression of IFN-β in human macrophages (26) and also exerted anti-fibrotic property in the hypochloric acid (HOCl) induced SSc-ILD mouse model (27). However, its effects on the IFN signature and on the efferocytosis capacities of macrophages have never been studied.

In this study, we explored the protective effects of the JAKi ruxolitinib in the bleomycin (BLM)-induced SSc-ILD in mice, with a special focus on IFN signature and associated effects.

We secondly analyzed the anti-fibrotic effects of ruxolitinib on human lung fibroblasts from patients with fibrotic ILD.

2. Materials and methods

2.1 Chemicals and reagents

Human recombinant cytokines IFN-γ, IFN-β and TGF-β1 were purchased from Peprotech (Neuilly sur Seine, France). Human recombinant M-CSF was obtained from Miltenyi Biotec SAS (Paris, France). Ruxolitinib (Ruxo, Hy-50856) and Bleomycin sulfate were provided by MedChemExpress, whereas camptothecin was purchased from Sigma-Aldrich (St-Quentin Fallavier, France). Antibodies (Ab) directed against: collagen I was from Southern Biotechnology Associates, Birmingham, AL, fibronectin (2413) was obtained from abcam, GAPDH (mab90009-P) was purchased from Covalab Bron France, α-SMA (clone 1A4) were from Sigma-Aldrich, phospho-smad2 (3104), smad2 (D43B4), phospho-smad3 (C25A9) and smad3 (C67H9), phospho-STAT3 (Tyr705), STAT3 were from Cell Signaling Technology (Ozyme, Montigny-le-Bretonneux, France).

2.2 Cell culture and treatments

2.2.1 Primary cultures of human macrophage:

Human macrophages were differentiated from peripheral blood monocyte. Briefly, buffy coat were obtained from healthy donors who gave a written consent for the use of blood samples for experimental research (Etablissement Français du Sang, Rennes, France). After a first separation by a Ficoll gradient centrifugation, the peripheral blood mononuclear cells were generated. The monocytes were isolated due to their adherence capacities and were differentiated into macrophages (M0) during 6 days in RPMI 1640 medium GlutaMAX (Gibco, Life technologies), containing 10 % heat-inactivated fetal bovine serum (FBS, Lonza, Levallois-Perret, France), 2 mM L-glutamine, 20 IU/mL penicillin, 20 µg/mL streptomycin

(ThermoFisher Scientific, Courtaboeuf, France) and 50 ng/ml of M-CSF. M0 were treated with 1 µM ruxolitinib and polarized in fresh RPMI 5 % FBS 10 ng/ml M-CSF supplemented with 20 ng/ml IFN-γ or IFN- β.

2.2.2 Primary cultures of human Lung Fibroblasts (HLFs):

Idiopathic pulmonary fibrosis (IPF)-HLFs were isolated from fibrotic lung tissue samples as previously described (28). The IPF samples were from patients undergoing open lung biopsy (mean age 64 year; range 57-75 years). IPF was diagnosed according to the ATS/ERS/JRS/ALAT criteria, including histopathological features of usual interstitial pneumonia (29). This study was approved by the local ethics committee (Ethics Committee CHU Rennes, no 16123). Written informed consent was obtained from all subjects. All experiments were performed in accordance with the World Medical Association declaration of Helsinki (30). Cell morphology of fibroblasts was checked by phase contrast microscopy.

IPF-HLFs (n=8) were cultured in Dulbecco's Modified Eagle Medium (DMEM) (Gibco™, Life Technologies, Courtaboeuf, France) supplemented with 10% fetal bovine serum (FCS) (Eurobio scientific, Evry, France), L-glutamine, antibiotic-antimycotic solution (Gibco™, Life Technologies) and used at passages 5 and 6. The IPF-HLFs were seeded in 6-well plates for 24 h, and starved in FCS-free DMEM for 16 h. TGF-β1-induced myofibroblast differentiation was measured by treating HLFs with 1µM ruxolitinib for 2 h and then with 1 ng/ml TGF-β1 for 24 h. The concentrations of ruxolitinib (1 µM) were in a comparable range to the maximal plasma concentrations (0,6 – 1,3 µM) that can be reached in patients treated with ruxolitinib (31).

2.3 Mouse model of BLM-induced systemic sclerosis

Male C57BL/6J mice weighing about 20 gr, used at 8 weeks of age, were acquired from Janvier Labs (Le Genest Saint Isle, France). Experimental scleroderma-associated ILD was induced by daily intradermal injections (ID) of 100 µl of BLM solution (at 0.4 mg/ml) into the shaved back of mice (5 days a week) for 4 weeks. Mice were randomly divided into 3 groups

of 6 mice each: ID of NaCl and oral solvent (0.5% Weight/Volume carboxymethyl glucose in NaCl 0.9%), ID of BLM dissolved in NaCl and oral solvent, ID of BLM and ruxolitinib (20 mg/kg, oral gavage twice a day). Animals were housed in similar autoclaved cages and fed food and water with identical housing condition. They were maintained under a 12/12h light/dark cycle, with controlled room temperature and humidity. Animal studies were reviewed and approved by the Committee on the Ethics of Animal Experiments under the French Ministry of Higher Education and Research (#17011-2018100812449655). The study was conducted in strict accordance with the recommendations in the Guide for the Care and Use of Laboratory Animals, EEC Council Directive 2010/63/EU.

2.4. Mouse model of HOCl-induced systemic sclerosis

Female C57BL/6J mice weighing between 18 and 20 gr, used at 8 weeks of age and purchased from Janvier Labs (Le Genest Saint Isle, France) were randomly divided into 2 groups: daily intradermal injections of 100 µl of PBS (n = 9) or HOCl (n = 8, one death due to biopsy sample procedure at week 3) as previously described (27). Animal studies were reviewed and approved by the Committee on the Ethics of Animal Experiments under the French Ministry of Higher Education and Research (permission#: 17011–2018100812449655).

2.5 Induction of apoptosis in Jurkat cells and quantification of efferocytosis in human macrophages

The human Jurkat cells CD4 T lymphocyte cell line was cultured in RPMI 1640 Glutamax medium supplemented with 10% of heat-inactivated FCS and antibiotics. Apoptosis was induced in Jurkat cells (Japo) through an exposure to 10 µM camptothecin for 4 h. The apoptosis was confirmed with FITC-Annexin V/iodide propidium staining using flow cytometry.

After labeling with 250 ng/mL pHrodo (IncuCyte® pHrodo® Red Cell Labeling Kit,Sartorius, Ann Arbor, USA), a pH-dependent fluorescent probe, the pHrodo^{+} apoptotic Jurkat cells were washed then add to macrophages (ratio 10/1) at 37°C. Quantification of engulfment of apoptotic

cells by macrophages was evaluated by measuring the intensity of the pHrodo red fluorescence emitted (560nm/585nm) in an acid medium of lysosomes, by fluorescence microscopy in real time (IncuCyte® live-cells Analysis system, Sartorius), with photographs carried out every 15 min for 3 h. The average fluorescence intensity (expressed as RCUxµm2/image) at 90 min was used to compare the level of efferocytosis between the different treatment conditions.

2.6 Sample collection for in vivo experiments

At the end of experimental procedure, mice were euthanized with an overdose of ketamine and xylazine (respectively at 120 and 20 mg/kg) and intracardiac exsanguination. Lungs were collected from each mouse and skin biopsies were performed using standardized biopsy punch near BLM injection sites. All samples were fixed in 10 % acetic acid formol for histopathological analyses or stored at −80 °C until used.

2.7 Hydroxyproline content in the skin

Collagen content in the skin was assessed using a colorimetric Hydroxyproline Kit Assay according to the manufacturer's protocol (BioVision, USA). Briefly, a skin punch of each mouse was homogenized in 100 µl of water and 100µl of NaOH (10 M) and hydrolyzed at 120°C for 1 h. The hydrolysate was secondly neutralized using equimolar adjunction of HCl (10 M). Then, a colorimetric product, visualized at 560 nm and proportional to the hydroxyproline content was generated using supplied regents, based on an oxidization reaction, allowing the quantification of hydroxyproline in skin punch for each mouse (27).

2.8 Histological analyses

2.8.1 Masson's trichrome, picrosirius-red staining: Skin and lung samples embedded in paraffin were sliced into serial 4 µm sections. Sections were then stained using Masson's trichrome or picrosirius-red staining. Slides were then scanned with the NanoZoomer 2.0 RS (Hamamatsu,

Tokyo, Japan). Images were captured for analysis using NDPview2 software (Hamamatsu). Skin thickness was evaluated by measuring the distance between the epidermal and the dermal–subcutaneous fat junction at a 10-fold magnification. Six random measurements per section were performed by a same blinded investigator and averaged for each section. The severity of fibrosis in Masson's trichrome stained lungs was quantified by the Ashcroft scoring system (33). Lung analyses were performed by a same investigator who was also blinded to the animal's group assignment

2.8.2 Caspase 3 apoptotic cell staining: Skin samples embedded in paraffin were dewaxing with EZ prep solution (DISCOVERY Wash) at 72°C. After washing with a reaction buffer, a liquid coverslip was automatically applied during all the IHC process to avoid drying of the slides. After cell conditioning with ultra CC1 solution and the inhibition of endogenous HRP with application of discovery inhibitor, a manual application of the anti-caspase3 cleaved (Asp175) antibody diluted with antibody diluent at 1/500 was performed. The slice was incubated during 60 min at 37°C followed by an automatic application of secondary antibody Omni Map anti-Rb HRP. The staining was visualized by automatic addition of the substrate (H_2O_2+purple) or (H_2O_2+DAB) and the HRP of the secondary antibody. A counter-staining with hematoxyline II during 16 min and Bluing Reagent during 4 min. After the IHC staining, the slides were washed with hot tap water and dishwasher gel to take away the oil of liquid coverslip. The slides were then dehydrated and mounted with Pertex mounting media.

2.9 Reverse transcription-quantitative polymerase chain reaction (RT-qPCR)

Total RNA was extracted from human cells and mouse tissue using the Nucleospin RNA Extraction Kit (Macherey-Nagel, Hoerdt, France) according to the manufacturer's instructions. RNA concentrations were measured by spectrofluorimetry using a NanoDrop 1000 (Thermo Fisher scientific) and was submitted to reverse transcription in complementary DNA (cDNA) using the High-Capacity cDNA Reverse Transcription Kit (Applied Biosystems, Thermo Fisher

Scientific). Quantitative PCR (qPCR) experiments were performed using the fluorescent probe SYBR Green methodology. Human and mouse predesigned KiCqStart® SYBR® Green primers for gene expression analysis were purchased from Sigma-Aldrich. PCR amplification was performed with the CFX384 Real-Time PCR detector (Bio-Rad Laboratories, Marnes-la-Coquette, France). The quantification of amplified genes was evaluated using the comparative cycle threshold (Cq) method (CFX Manager Software). Mean of Cq values were used to normalize expression of the steady-state target mRNA levels to those of the 18S ribosomal protein, using the $2(-\Delta\Delta Cq)$ method. It is noted that some samples of mouse tissues were not obtained in a sufficient quantity to evaluate the expression of all the genes of interest.

2.10 Western Blotting

Total IPF-HLF extract was lysed in ice-cold RIPA buffer containing 150 mM NaCl, 50 mM Tris-HCl, 0,1 % SDS, 1 % Triton X-100, 0,5 % Na deoxycholate, 50 mM sodium fluoride, 5 mM EDTA, 0,5 mM dithiotréitol, 1X protease inhibitor cocktail (Roche Diagnostic, Meylan, France) and phosphatase inhibitor cocktail 2, phosphatase inhibitor cocktail 3 (Sigma-Aldrich). The lysate was centrifuged at 17900g for 30 min. The supernatant protein was denatured by heated for 5 min at 95°C in a loading buffer (glycerol 25 %(V/V), 0,3 % bromophenol (V/V), 10 % SDS (V/V), 0,5 M Tris pH 6,8 and 5 % β mercaptoetanol) and protein concentration was determined using the Bio-Rad Protein Assay Kit. 35µg of protein was separated by 10% SDS-PAGE and transferred overnight (30V at 4°C) into nitrocellulose membrane (Pall Corporation). Immunoblot were blocked with T-TBS (0,5 M Tris pH 7,4, 1,5 M NaCl, Tween-20 0,1 %(V/V)) containing 4% of bovine serum albumin, were then hybridized overnight at 4°C with appropriate primary antibodies (1/1000) and, after washing, were incubated with horseradish peroxidase-conjugated secondary antibodies (1/2000) before analysis by chemiluminescence.

The densitometry of blots was measured using the Image Lab™ Software for total protein normalization (Bio-Rad) and normalized to GAPDH.

2.11 Statistical analyses

Data were presented as means ± standard error on the mean (SEM). Comparisons between more than 2 groups were performed by repeated measure analysis of variance for paired or one-way analysis of variance followed by Dunnett's multiple comparison post-hoc tests for independent groups. Depending on conditions and Gaussian distribution, Student's t test, paired-t-test or Mann and Whitney test were used to compare 2 groups. A p-value < 0.05 was considered significant. Data analyzes were performed with GraphPad Prism 5.0 software (GraphPad Software, La Jolla, CA, USA).

3. Results

3.1 BLM- and HOCl-induced skin thickness is associated with an increase of apoptotic cells and an interferon signature

Histological changes and skin thickness was significantly increased in BLM and HOCl mouse models (Fig 1A). These changes were associated with a significant increase of cleaved caspase-3 positive cells, reflecting an increase of dermal apoptosis (Fig 1B). mRNA expression of ISGs such as the chemokine CXCL10, Ifi44 or the transcription factor IFR3 was significantly increased in both mouse models (Fig 1C). The accumulation of dermal apoptotic cells could be related to an IFN-dependent decreased of efferocytosis.

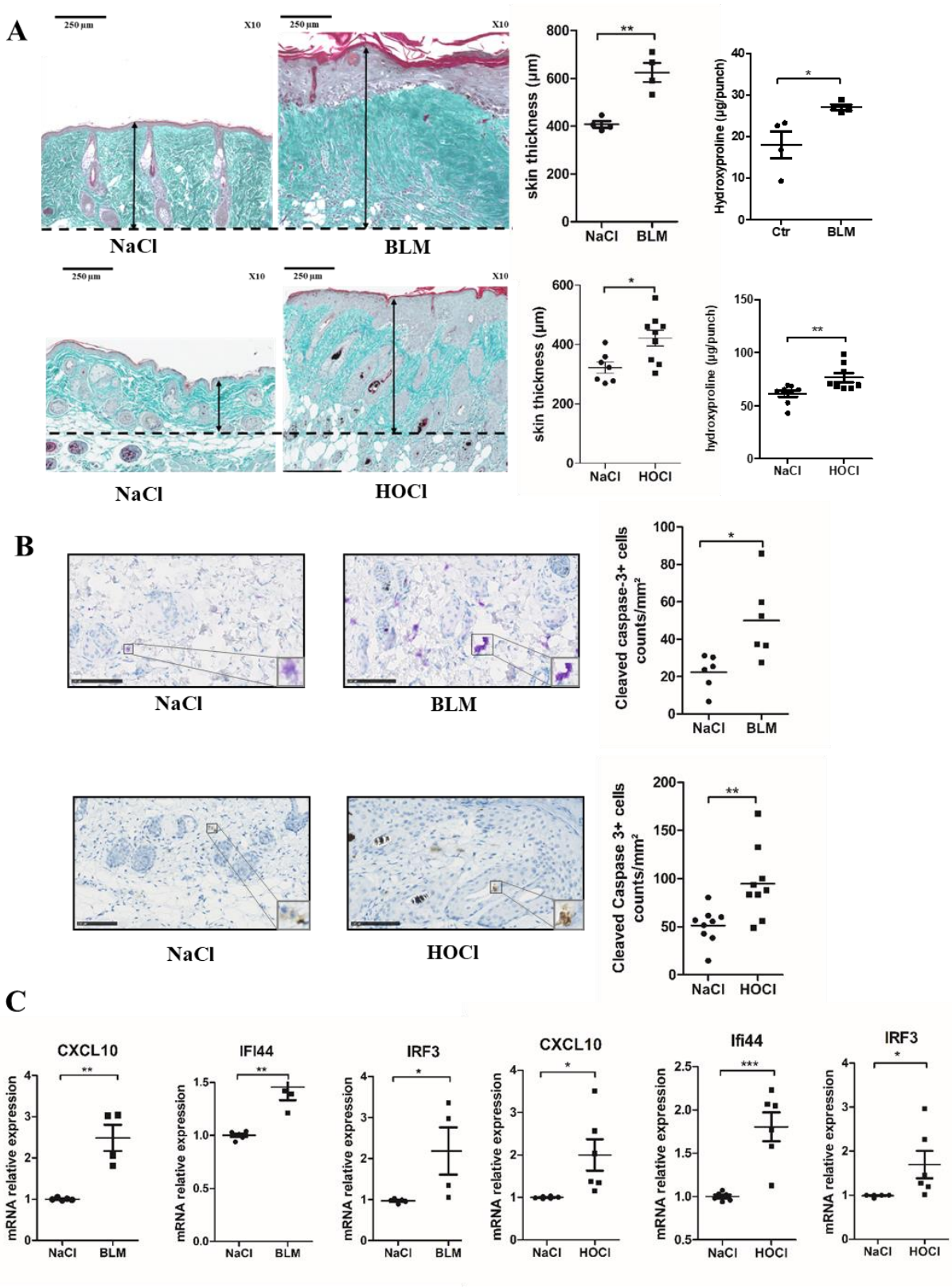

Fig.1. **Skin thickness, apoptosis and IFN signature in two systemic mouse SSc models.**

A) Evaluation of skin thickness and hydroxyproline content in BLM and HOCl SSc-mouse models. C57BL/6 mice were intradermally injected with BLM, HOCl or saline every day for 4 weeks (BLM) or for 6 weeks (HOCl). Skin paraffin sections were stained according to the Masson's trichrome staining protocol. Data of skin thickness (µm,

6 measures per mice) are expressed by the means +/- SEM (n = 6-9 mice per group). The quantification of hydroxyproline content (µg/punch) is expressed by the means ± SEM (n = 4 to 7 mice per group); p value was calculated with Student's t-test, * p< 0.05; ** p< 0.01 versus NaCl group. B) Evaluation of apoptotic cell number in dermal skin of BLM and HOCl SSc-mouse models. Skin sections were stained according to cleaved Caspase 3 stain protocol. Data corresponding to the number of apoptotic cells are expressed by the means +/- SEM of (n = 6-9 mice per group), p value was calculated with Student's t-test, ** p< 0.01 versus NaCl group. C) Evaluation of IFN signature in skin of BLM and HOCl mouse models. The mRNA relative expressions of three ISGs are expressed as means +/- SEM (n=3 to 7 mice per group) with BLM or HOCl group arbitrarily set to 1. * p< 0.05; ** p< 0.01; *** p< 0.001 expressing differences between the group HOCl or BLM with saline group.

3.2 Ruxolitinib improves efferocytosis capacity of human macrophages exposed to IFN-β and IFN-γ.

To assess the effect of ruxolitinib on efferocytosis, human monocyte-derived-macrophage (MDM) were treated with 1 µM ruxolitinib and polarized into pro-inflammatory macrophages by adding IFN-β or IFN-γ, they were then exposed to pHRodo-labeled apoptotic Jurkat cells. IFN-β- or IFN-γ-polarized MDM showed a decreased of the percentage of pHRodo$^+$ engulfed cells, with a strongest effect onto IFN-γ-treated MDM (almost 50% reduction) (Fig 2). Efferocytosis levels were restored by ruxolitinib in the both IFN-treated macrophages (Fig 2). A decreased phosphorylation of STAT1 in IFN-treated MDM after ruxolitinib treatment was previously validated (27).

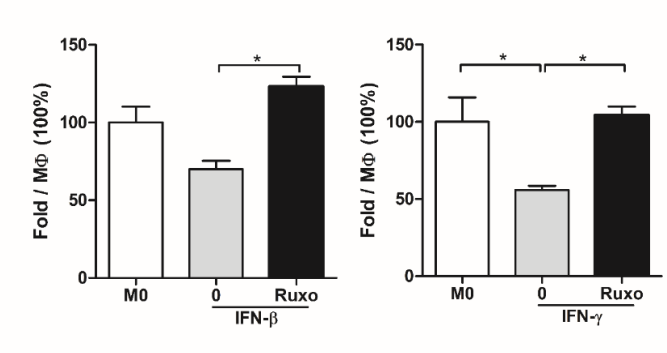

Fig 2. Ruxolitinib improves efferocytosis capacity of human macrophages exposed to IFN-β or IFN-γ
Efferocytosis capacities of monocyte-derived macrophages (MDM) exposed or not to IFN-β or IFN-γ (20 µg/ml) in the presence or not of ruxolitinib (Ruxo) at 1 µM were evaluated by measuring the intensity of the pHrodo red fluorescence. Efferocytosis of untreated macrophages (M0) used as control was set as 100%. Experiments were conducted in MDM from n≥ 4 independent healthy donors and are expressed as means ± SEM. p value was calculated with ANOVA Dunnet test, *p< 0.05.

3.3 Ruxolitinib improves skin and lung parameters induced in BLM-SSc mouse model

We next analyzed ruxolitinib effects on skin and lung tissues of BLM-SSc mouse model. The increased of skin thickness (Fig 3A) and of hydroxyproline content (Fig 3B) observed in BLM exposed mice were both significantly reduced by ruxolitinib. Ruxolitinib also significantly decreased the number of cleaved caspase-3 cells in the dermis (54.52% in BLM vs 25.83% in BLM+Ruxo, $p<0.01$) (Fig 3C) suggesting either a protective effect of ruxolitinib on BLM-induced cell apoptosis or an improvement of apoptotic cell clearance by ruxolitinib.

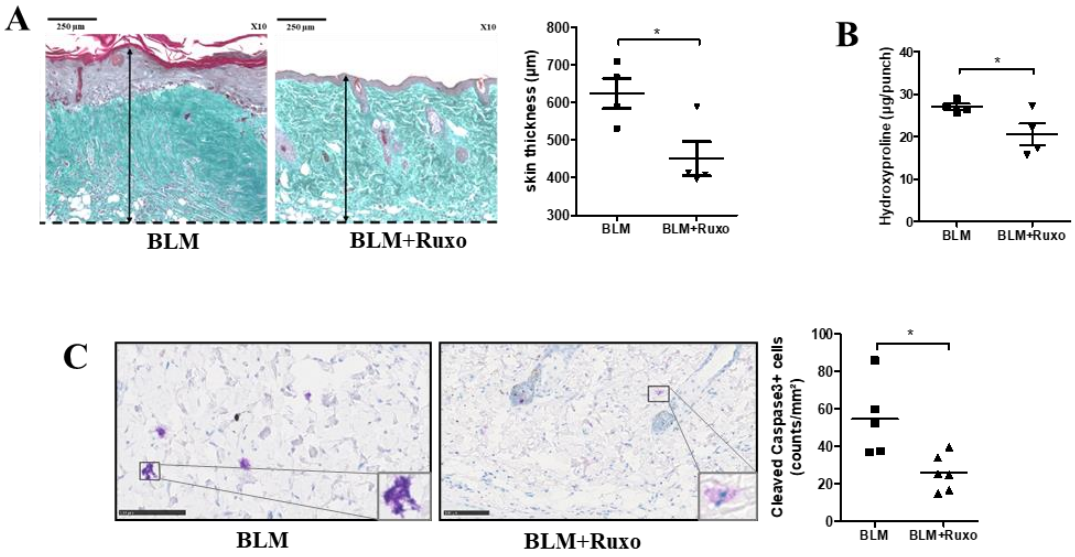

Fig 3. Ruxolitinib improves skin parameters induced in BLM-SSc mouse model

(A) Skin thickness, measured on paraffin sections stained to Masson's trichrome, is expressed in µm. Data represent the means ± SEM of 6 measures per skin section for each 4 mice per group. p value was calculated with Student's t-test, * $p<0.05$. (B) Skin fibrosis was evaluated by the quantification of hydroxyproline content (µg/punch) which is expressed by the means ± SEM (n = 4 mice per group). p value was calculated with Student's t-test, * $p<0.05$. (C) Dermal cell apoptosis was evaluated on skin sections stained to an anti-cleaved Caspase 3 antibody. Data expressed by the count of caspase 3 positive cells/mm^2 represented the means ± SEM (n = 6 mice per group). p value was calculated with Student's t-test, * $p<0.05$.

The histopathological analysis of lung tissue reveals that ILD induced by BLM was decreased by ruxolitinib (Supplementary Fig. S1). Similarly, collagen deposit assessed by the Sirius red staining (Fig 4A) and lung fibrosis assessed by Ashcroft score (Fig 4B) in BLM-SSc mice, were reduced, although moderately, in ruxolitinib treated mice. The positive effects of

ruxolitinib on BLM-induced lung fibrosis were also confirmed by a significant mRNA down-expression of typical profibrotic genes (Acta2, COL1A1, COL3A1, Fn1, TGF-β) in comparison with the BLM group (Fig 4C). Otherwise, the mRNA expressions of the IFN-responsive genes, CXCL10, Ifi44, and IRF3 in the lung were significantly increased in BLM- in comparison to NaCl-exposed mice (Fig 4D). Among these three ISGs, only Ifi44 mRNA expression was significantly reduced in the presence of ruxolitinib in comparison to BLM group (Fig 4D). As fibroblasts are the key cells producing extracellular matrix proteins, we next explored the effects of ruxolitinib on human lung fibroblasts.

Figure 4

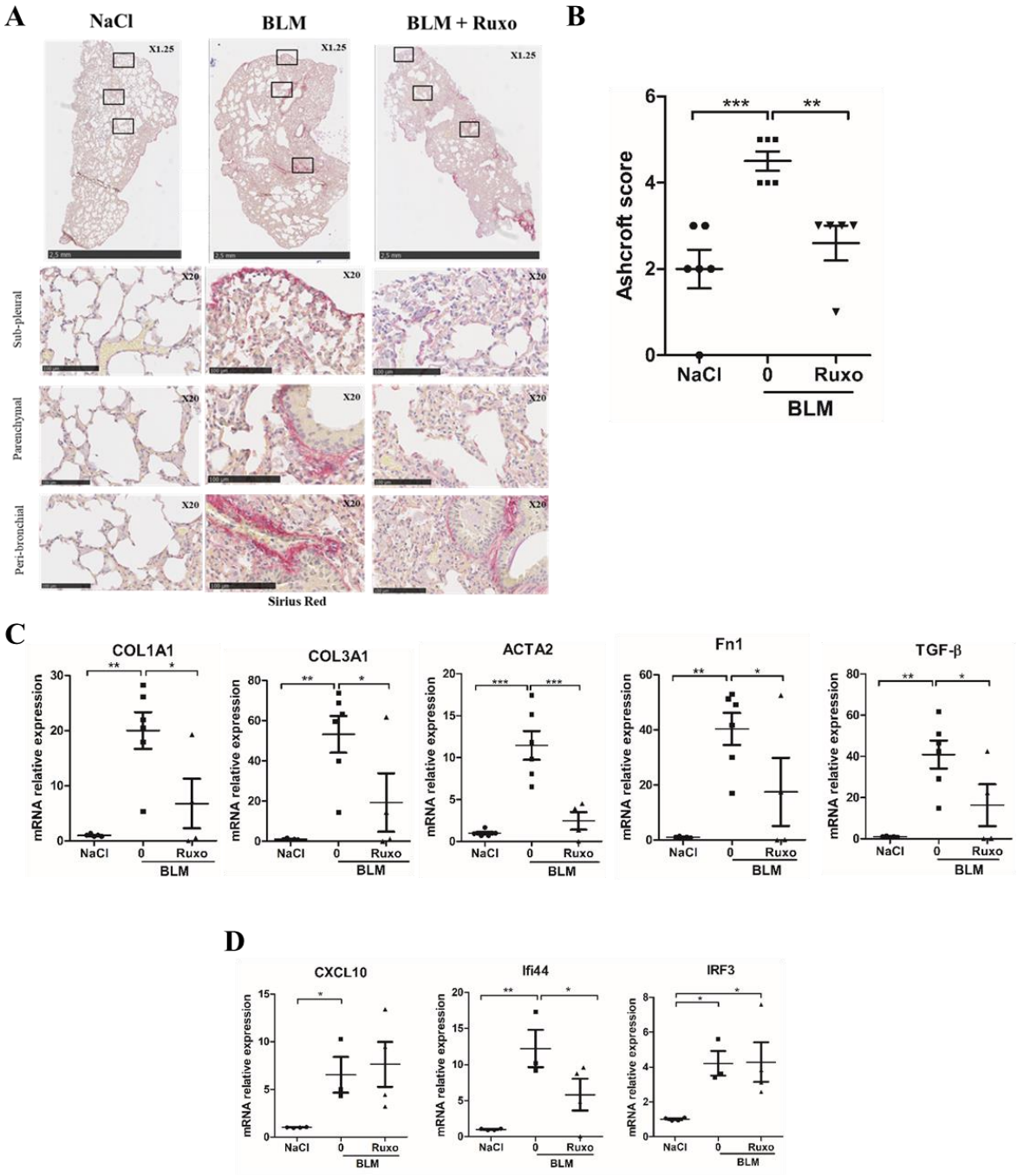

Fig.4. Ruxolitinib improves lung parameters induced in BLM-SSc mouse model

(A) Staining of lung (left upper lobe) showing total section (x1,25) and details of the sub-pleural, parenchymal and peri-bronchial regions (x20) by Sirius red. Sections of mouse lung are representative of each group (n = 6 mice per group). Ashcroft score (B) and the mRNA relative expressions of key pro-fibrotic markers (C) and of three ISGs (D) in the lungs are expressed as the means ± SEM in comparison with the BLM group. p value was calculated with ANOVA followed by Newman-Keuls multiple comparison post-hoc test. * $p<0.05$; ** $p< 0.01$; *** $p<0.001$ (n = 3 to 6 mice per group).

3.4 The antifibrotic properties of ruxolitinib may be related to its direct impact on human lung fibroblasts

The impact of ruxolitinib on human fibroblasts was evaluated in idiopathic pulmonary fibrosis-human lung fibroblasts (IPF-HLF), as IPF is a prototypical fibrotic lung disease sharing many similarities with SSc-ILD, in terms of pathogenesis and treatment strategy. It is noted that the effect of ruxolitinib has been not tested on TGF-β1-induced control fibroblasts in this study as the basal expression levels of fibrotic markers in control fibroblasts were previously demonstrated to be similar to IPF-HLF (28). Incubation of IPF-HLF with 1 ng/ml of TGF-β1 for 24 h significantly up-regulated mRNA expressions of pro-fibrotic genes (Col1A1, Col3A1, Col4A2, Serpin, Fn1 and ACTA2) and ruxolitinib exposure prevented the over-expression of all these typical TGF-β-activated fibroblast markers except for Fn1 mRNA expression (Fig 5A). Moreover, ruxolitinib significantly reduced α-SMA protein expression and tended to reduce collagen-1 but not fibronectin protein levels in TGF-β-activated IPF-HLFs (Fig 5B and 5C), suggesting that improvement of ILD by ruxolitinib could be related to its effects on lung fibroblasts. Ruxolitinib significantly decreased TGF-β1-induced phosphorylation of SMAD2 and SMAD3 proteins (Fig 6A and 6B) but also decreased TGF-β1-induced phosphorylation of STAT3 (Fig 6C), supporting that ruxolitinib could directly limit the profibrotic properties of human lung fibroblast *in vitro* by targeting both canonical and non-canonical TGF-β signaling pathways.

Figure 5

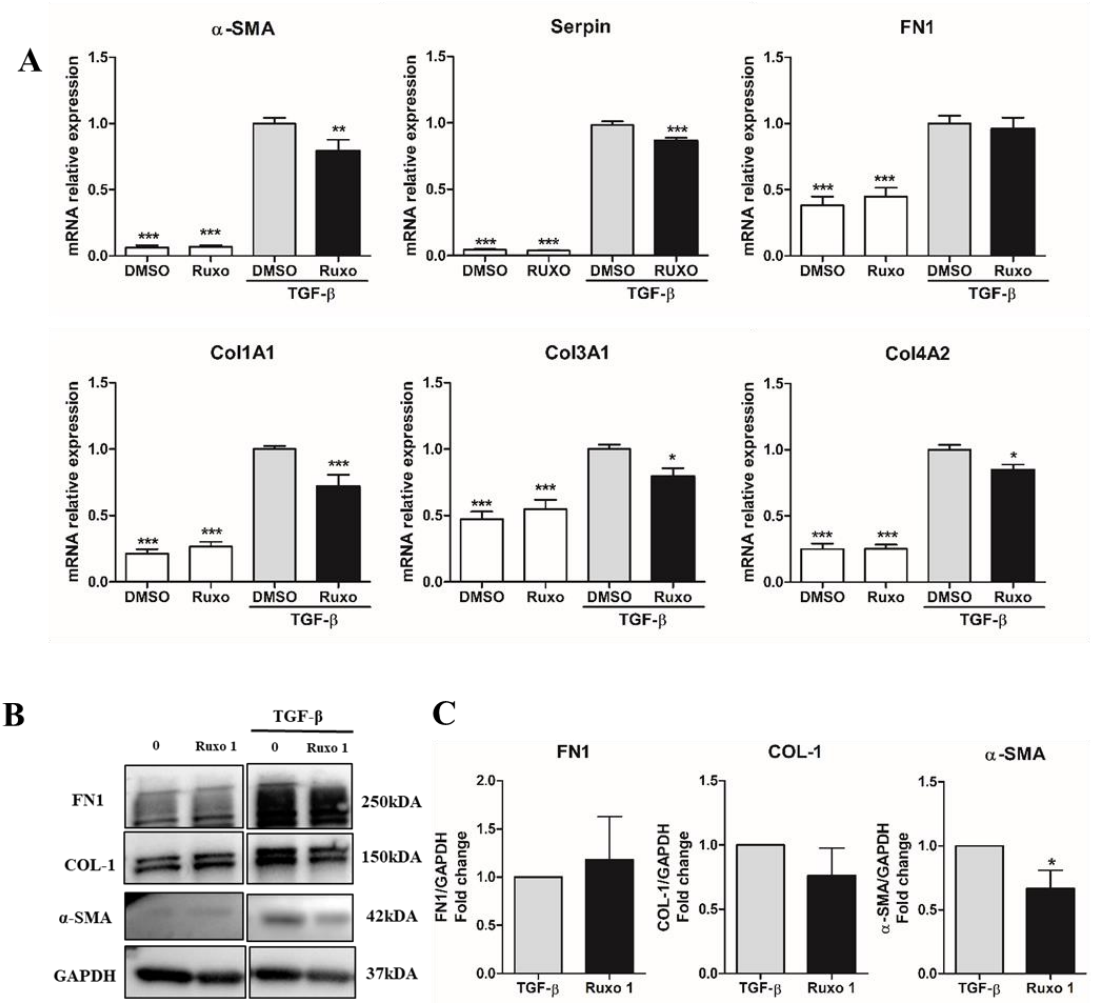

Fig.5. Ruxolitinib tends to decrease TGF-β-induced cell differentiation in IPF-HLF

(A) The mRNA relative expression in IPF-HLFs stimulated by TGF-β and treated or not with 1 μM of Ruxo was determined by arbitrarily setting at 1 mRNA concentrations measured in TGF-β treated cells. Results are expressed as with means ± SEM of 8 independent experiments. Significant differences were determined by ANOVA followed by Dunnett's multiple comparison t-test, * $p<0.05$; ** $p< 0.01$; *** $p<0.001$. (B) Representative Western blots of fibronectin (Fn1), collagen-1 (COL-1) and α-SMA in IPF-HLFs treated with 1 μM Ruxo for 24 h and then stimulated with 1 ng/ml TGF-β1 for 24 h. (C) Proteins were quantified by densitometry and normalized to GAPDH expression. The fold change in protein expression in stimulated cells was determined by arbitrarily setting at 1 the protein expression measured in TGF-β treated cells. Results are expressed as the means ± SEM of 8 IPF-HLF independent cell culture experiments. Significant differences were determined by ANOVA followed by the Dunnett's multiple comparison t-test, * $p<0.05$.

Figure 6

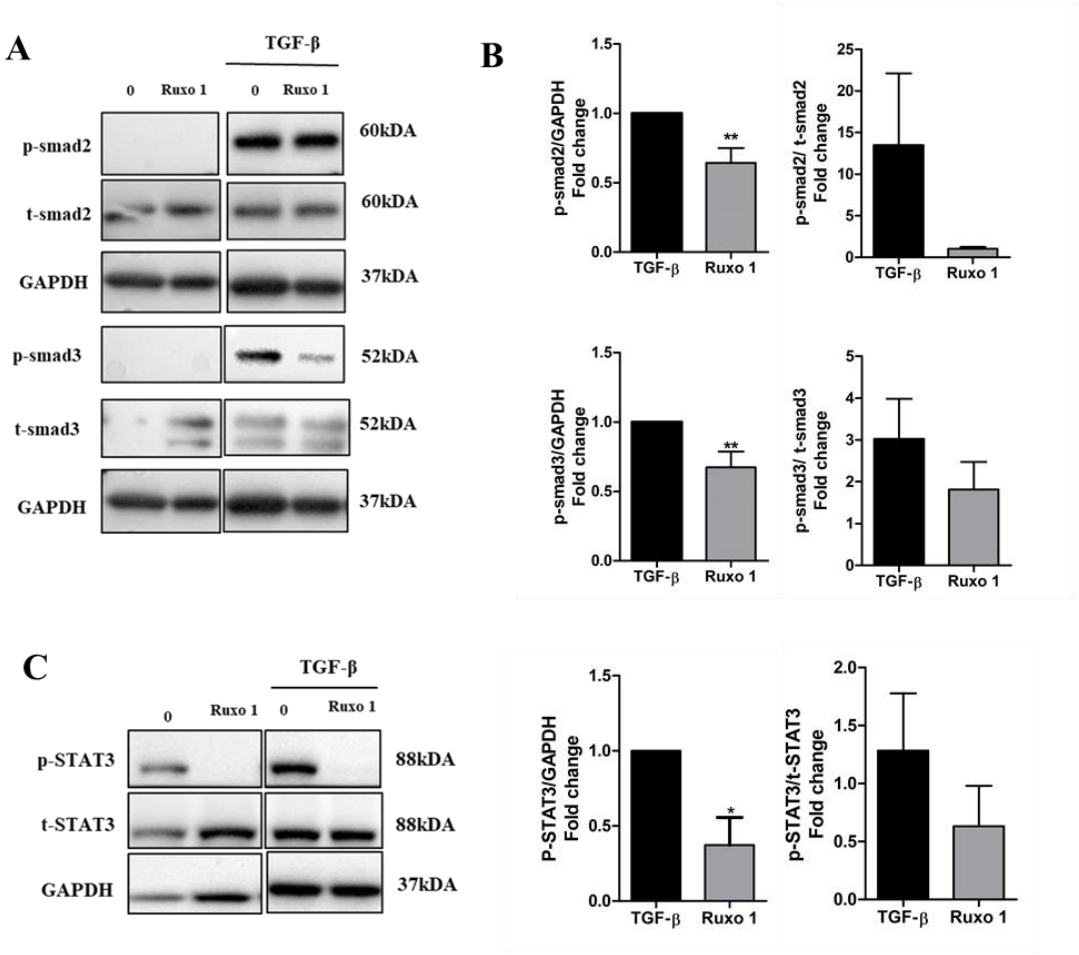

Fig.6. Ruxolitinib prevents the phosphorylation of SMAD2/3 induced by TGF-β in IPF-HLFs

(A) Representative Western blots showing the phosphorylation of SMAD2 and SMAD3 in IPF-HLFs treated with 1 μM Ruxo for 24 h and then stimulated with 1 ng/ml TGF-β for 24 h. (B) Proteins were quantified by densitometry and then normalized to the GAPDH expression. The fold change in protein expression in stimulated cells was determined by arbitrarily setting at 1 the protein expression measured in TGF-β treated cells. Results are expressed as with means ± SEM of 8 IPF independent cell culture experiments. (C) Representative Western blots showing the phosphorylation of STAT3 and protein quantification and normalization to GAPDH expression by densitometry. The fold change in protein expression in stimulated cells was determined by arbitrarily setting at 1 the protein expression measured in TGF-β treated cells. Results are expressed as with means ± SEM of 4 IPF independent cell culture experiments. Significant differences were determined by ANOVA followed by the Dunnett's multiple comparison t-test, * $p< 0.05$; ** $p< 0.01$.

4. Discussion

In this study, we demonstrated anti-fibrotic effects of the pan-JAKi ruxolitinib in the skin and the lung of BLM induced-SSc-ILD model and in TGF-β-induced lung fibroblasts isolated from patients with IPF. IFN signature and the presence of apoptotic cells in skin tissues were associated with dermal thickness in BLM- and HOCl-induced SSc-ILD mouse model.

Our study demonstrated that the non-selective JAKi ruxolitinib improved skin histological changes and dermal thickness induced by BLM-intradermal injections. These skin effects of ruxolitinib have also been observed in previous publications based on other SSc-ILD models (27,34), confirming the positive effects of pan-JAKi on SSc-related fibrosis. Skin fibrosis was associated with an increase of apoptotic cells in the dermis of BLM- induced SSc model (35), in the genetic Fra-2 SSc mouse model (36) and also, as we demonstrated in this article, in the HOCl-induced SSc model; therefore showing that the presence of apoptotic cells in dermis is a common feature of skin fibrosis in SSc. In human skin, apoptotic cells were mostly identified as endothelial cells and not as immune cells (13). Although we have not characterized the nature of these apoptotic cells in our study, their absence of co-localization with vessels does no support an endothelial origin. Additional immuno-histological experiments will be required to fully characterize their nature. In the BLM-induced SSc model, induction of apoptosis occurs via the Fas/Fas ligand pathway (35), and interestingly, the reduction of skin fibrosis and collagen deposition is associated with the reduction of cellular apoptosis (37). These results are consistent with ours, as the reduction of apoptotic cell number by ruxolitinib is associated with skin fibrosis improvement as assessed by dermal thickness and the level of hydroxyproline. Altogether, these data support a contribution of cell death to skin remodeling and suggest that the positive effects of ruxolitinib on skin fibrosis may be related, at least in part, to its ability to limit the presence of apoptotic cells in the dermis.

In agreement with our previous results in the HOCl induced-SSc model, the pan-JAKi ruxolitinib decreases pulmonary fibrosis assessed by Sirius red and the expression of fibrosis markers. This result is in agreement with those of Zhang et al, which demonstrates that ruxolitinib has decreased pulmonary fibrosis and the differentiation of fibroblasts into myofibroblasts in the intratracheal instillation model of BLM (34). This anti-fibrotic effect of ruxolitinib can also be explained by the inhibition of the JAK-STAT signaling pathways driving macrophage polarization as this JAKi reduced the expression of some pro-inflammatory (or M1) and pro-fibrotic (or M2a) macrophage-associated markers in the HOCl mouse model (27). Analysis of blood and tissues of SSc patients as well as in HOCl-SSc mouse model showed a mixed phenotype of M1/M2 (27,38). The latter is associated with SSc-ILD and thus the severity of the disease (39). SSc patients also exhibit an IFN signature in the very early phase (14,40) concomitantly with a potentially IFN mediated-M1 macrophage signature in skin tissue of human (40) or HOCl-SSc mice (27). These data suggest that M1 activation and concomitant IFN signature are hallmarks of early SSc.

In our study, we showed a decrease in efferocytosis capacity of human macrophages exposed to IFN-β- or IFN-γ. This result is in agreement with those obtained in M1 macrophages (41) and could explain the defect in efferocytosis observed in macrophages of SSc patients (12) as an IFN signature was also described in peripheral blood mononuclear cells (42). This hypothesis is in accordance with the defect of efferocytosis observed in other systemic autoimmune diseases characterized by a high IFN signature such as systemic lupus (43).

The pulmonary anti-fibrotic effect of ruxolitinib cannot be fully explained by its action on the IFN signature. Indeed, only Ifi44 mRNA lung expression was decreased in the presence of ruxolitinib in comparison to BLM group. This was not the case in the HOCl induced SSc-ILD model where CXCL10 and IRF3 expression were decreased by ruxolitinib but at early phase (27). Additional experiments in the early phase might provide some answers (44).

Beyond macrophages, fibroblasts are the other key cells involved in the pathogenesis of SSc. Similarly to skin fibroblasts of SSc patients, IPF lung fibroblasts strongly express JAK2 and STAT3 in comparison with control fibroblasts (45), and treatments targeting fibroblasts initially approved in IPF-ILD have also been recently approved in SSc-ILD (46), suggesting common activation mechanisms in these two fibrotic diseases. By contrast with IPF, lung biopsy is rarely performed in SSc-ILD and SSc-lung fibroblasts are rarely available. In our study, we used IPF-HLFs and demonstrated a decrease of STAT3 phosphorylation by ruxolitinib supporting an efficacy of JAKi also via the non-canonical pathway (47). The anti-fibrotic effects of ruxolitinib could also be attributed to a decrease of type I-IFN/IFNAR/IRF7/SMAD3 signaling as both IRF7 mRNA and protein are overexpressed in SSc skin fibroblasts (48). Wu et al. showed a colocalization of IRF7 and SMAD3 in SSc fibroblasts and demonstrated that TGF-β-induced collagen and fibronectin expressions were significantly decreased in cells transfected with siRNA IRF7 (48). The decrease of several TGF-β-induced fibrotic markers by ruxolitinib may be explained by its capacity to reduce the canonical signaling pathway involving SMAD2 and 3 along with an impact on the non-canonical pathway. In accordance with this hypothesis, the JAK2 inhibitor TG101209 that reduced fibrotic markers in TGF-β-exposed healthy skin human fibroblasts was not efficient in fibroblast nucleofected with Jak2 siRNA, suggesting that a non-canonical pathway involving phospho-Jak2 was activated by TGF-β in skin fibroblasts and that this JAK pathway may be an promising therapeutic target (47,49). Such data were also supported by the efficiency of ruxolitinib to reduce fibrotic markers expression in skin fibroblasts (34). Altogether, these data suggest a link between inflammation illustrated by the IFN/JAK/STAT signaling pathway and fibrosis, characterized by TGF-β signaling pathway, in lung fibroblasts from patients with chronic ILD such as IPF or SSc. Examining the effects of ruxolitinib in TGF-β and IFN co-treated lung fibroblasts on the p-SMAD3 and IRF3 interaction may help to confirm these results in the future. Nonetheless, comparing signaling pathways of

skin tissues with lung tissues in a same disease or of lung samples from two fibrotic diseases can be hazardous as divergent patterns of IFN signaling have been described (50).

In this study, we demonstrated that ruxolitinib has prevented the increase of apoptotic cell number and confirmed the anti-fibrotic effects of ruxolitinib *in vivo* in a systemic SSc mouse model and *in vitro* in human lung fibroblasts. Overall, our results strengthened the relevance of using JAKi as a therapeutic approach for skin and lung manifestations of SSc, a systemic autoimmune disease without efficient disease modifying drug available for all patients to date.

Author Contributions

Design of the study: NB, AL, VL. Acquisition of the data: NB, ML, AL, ELT. Interpretation of the data: NB, AL, VL. Manuscript preparation: NB, AL, VL. Provided essential materials: AJ, SJ, LV.

Declaration of competing interest:

Outside the submitted work, Stéphane Jouneau has received fees, funding or reimbursement for national and international conferences, boards, expert or opinion groups, research projects over the past 3 years from AIRB, Bellorophon Therapeutics, Biogen, Boehringer, Chiesi, Fibrogen, Galecto Biotech, Gilead, LVL, Novartis, Olam Pharm, Pfizer, Pliant Therapeutics, Roche, Sanofi- Genzyme, Savara.

The other authors have no conflict to interest to declare.

Data availability

Data will be made available on request.

Acknowledgements

The authors thank the animal house facilities (ARCHE), the platform of Flow cytometry and the Platform of Histo-Pathology Hight Precision (H_2P_2) (Biosit, Rennes, France). This work was supported by the Institut National de la Santé et de la Recherche Médicale (INSERM), the Université de Rennes (Univ Rennes) and the "Groupe francophone de recherche sur la sclérodermie".

Appendix A: Supplementary data

Supplementary data are available

References

1. Perelas A, Silver RM, Arrossi AV, Highland KB. Systemic sclerosis-associated interstitial lung disease. Lancet Respir Med. mars 2020;8(3):304-20.

2. Asano Y. Systemic sclerosis. J Dermatol. févr 2018;45(2):128-38.

3. Brown M, O'Reilly S. The immunopathogenesis of fibrosis in systemic sclerosis. Clinical and Experimental Immunology. 2018;12.

4. Lescoat A, Lecureur V, Varga J. Contribution of monocytes and macrophages to the pathogenesis of systemic sclerosis: recent insights and therapeutic implications. 2021;33(6):8.

5. Mahoney JM, Taroni J, Martyanov V, Wood TA, Greene CS, Pioli PA, et al. Systems level analysis of systemic sclerosis shows a network of immune and profibrotic pathways connected with genetic polymorphisms. PLoS Comput Biol. janv 2015;11(1):e1004005.

6. Taroni JN, Greene CS, Martyanov V, Wood TA, Christmann RB, Farber HW, et al. A novel multi-network approach reveals tissue-specific cellular modulators of fibrosis in systemic sclerosis. Genome Med. 23 mars 2017;9(1):27.

7. Hinchcliff M, Toledo DM, Taroni JN, Wood TA, Franks JM, Ball MS, et al. Mycophenolate Mofetil Treatment of Systemic Sclerosis Reduces Myeloid Cell Numbers and Attenuates the Inflammatory Gene Signature in Skin. J Invest Dermatol. juin 2018;138(6):1301-10.

8. Huang J, Maier C, Zhang Y, Soare A, Dees C, Beyer C, et al. Nintedanib inhibits macrophage activation and ameliorates vascular and fibrotic manifestations in the Fra2 mouse model of systemic sclerosis. Annals of the Rheumatic Diseases. 1 nov 2017;76(11):1941-8.

9. Stochmal A, Czuwara J, Trojanowska M, Rudnicka L. Antinuclear Antibodies in Systemic Sclerosis: an Update. Clinic Rev Allerg Immunol. 1 févr 2020;58(1):40-51.

10. Tiniakou E, Crawford J, Darrah E. Insights into origins and specificities of autoantibodies in systemic sclerosis. Current Opinion in Rheumatology. nov 2021;33(6):486-94.

11. Kawano M, Nagata S. Efferocytosis and autoimmune disease. Int Immunol. 14 nov 2018;30(12):551-8.

12. Ballerie A, Lescoat A, Augagneur Y, Lelong M, Morzadec C, Cazalets C, et al. Efferocytosis capacities of blood monocyte-derived macrophages in systemic sclerosis. Immunology & Cell Biology. 2019;97(3):340-7.

13. Maehara T, Kaneko N, Perugino CA, Mattoo H, Kers, J, Allard-Chamard H, et al. Cytotoxic CD4+ T lymphocytes may induce endothelial cell apoptosis in systemic sclerosis. Journal of Clinical Investigation. 6 avr 2020;130(5):2451-64.

14. Tan FK, Zhou X, Mayes MD, Gourh P, Guo X, Marcum C, et al. Signatures of differentially regulated interferon gene expression and vasculotrophism in the peripheral blood cells of systemic sclerosis patients. Rheumatology. 1 juin 2006;45(6):694-702.

15. Brkic Z, van Bon L, Cossu M, van Helden-Meeuwsen CG, Vonk MC, Knaapen H, et al. The interferon type I signature is present in systemic sclerosis before overt fibrosis and might contribute to its pathogenesis through high BAFF gene expression and high collagen synthesis. Ann Rheum Dis. août 2016;75(8):1567-73.

16. Assassi S, Swindell WR, Wu M, Tan FD, Khanna D, Furst DE, et al. Dissecting the Heterogeneity of Skin Gene Expression Patterns in Systemic Sclerosis. Arthritis & Rheumatology. 2015;67(11):3016-26.

17. Skaug B, Assassi S. Type I interferon dysregulation in Systemic Sclerosis. Cytokine. août 2020;132:154635.

18. Assassi S, Mayes MD, Arnett FC, Gourh P, Agarwal SK, McNearney TA, et al. Systemic sclerosis and lupus: Points in an interferon-mediated continuum. Arthritis & Rheumatism. 2010;62(2):589-98.

19. Liu X, Mayes MD, Tan FK, Wu M, Reveille JD, Harper BE, et al. Correlation of interferon-inducible chemokine plasma levels with disease severity in systemic sclerosis. Arthritis & Rheumatism. 2013;65(1):226-35.

20. Christmann RB, Sampaio-Barros P, Stifano G, Borges CL, de Carvalho CR, Kairalla R, et al. Association of Interferon- and Transforming Growth Factor β–Regulated Genes and Macrophage Activation With Systemic Sclerosis–Related Progressive Lung Fibrosis. Arthritis & Rheumatology. 2014;66(3):714-25.

21. Jiang J, Zhao M, Chang C, Wu H, Lu Q. Type I Interferons in the Pathogenesis and Treatment of Autoimmune Diseases. Clinic Rev Allerg Immunol. 1 oct 2020;59(2):248-72.

22. Ciechomska M, Skalska U. Targeting interferons as a strategy for systemic sclerosis treatment. Immunology Letters. 1 mars 2018;195:45-54.

23. Guo X, Higgs BW, Bay-Jensen AC, Karsdal MA, Yao Y, Roskos LK, et al. Suppression of T Cell Activation and Collagen Accumulation by an Anti-IFNAR1 mAb, Anifrolumab, in Adult Patients with Systemic Sclerosis. Journal of Investigative Dermatology. 1 oct 2015;135(10):2402-9.

24. Gadina M, Le MT, Schwartz DM, Silvennoinen O, Nakayamada S, Yamaoka K, et al. Janus kinases to jakinibs: from basic insights to clinical practice. Rheumatology. 1 févr 2019;58(Supplement_1):i4-16.

25. Escamilla Gómez V, García-Gutiérrez V, López Corral L, García Cadenas I, Pérez Martínez A, Márquez Malaver FJ, et al. Ruxolitinib in refractory acute and chronic graft-versus-host disease: a multicenter survey study. Bone Marrow Transplant. mars 2020;55(3):641-8.

26. Febvre-James M, Lecureur V, Augagneur Y, Mayati A, Fardel O. Repression of interferon β-regulated cytokines by the JAK1/2 inhibitor ruxolitinib in inflammatory human macrophages. International Immunopharmacology. 1 janv 2018;54:354-65.

27. Lescoat A, Lelong M, Jeljeli M, Piquet-Pellorce C, Morzadec C, Ballerie A, et al. Combined anti-fibrotic and anti-inflammatory properties of JAK-inhibitors on macrophages in vitro and in vivo: Perspectives for scleroderma-associated interstitial lung disease. Biochemical Pharmacology. 1 août 2020;178:114103.

28. Joannes A, Morzadec C, Duclos M, Gutierrez FL, Chiforeanu DC, Le Naoures C, et al. Arsenic trioxide inhibits the functions of lung fibroblasts derived from patients with idiopathic pulmonary fibrosis. Toxicology and Applied Pharmacology. avr 2022;441:115972.

29. Raghu G, Remy-Jardin M, Myers JL, Richeldi L, Ryerson CJ, Lederer DJ, et al. Diagnosis of Idiopathic Pulmonary Fibrosis. An Official ATS/ERS/JRS/ALAT Clinical Practice Guideline. Am J Respir Crit Care Med. sept 2018;198(5):e44-68.

30. World Medical Association Declaration of Helsinki: Recommendations Guiding Physicians in Biomedical Research Involving Human Subjects. JAMA. 19 mars 1997;277(11):925-6.

31. Ogawa Y, Ogura M, Suzuki T, Ando K, Uchida T, Shirasugi Y, et al. A phase I/II study of ofatumumab (GSK1841157) in Japanese and Korean patients with relapsed or refractory B-cell chronic lymphocytic leukemia. Int J Hematol. 1 août 2013;98(2):164-70.

32. Lescoat A, Ballerie A, Lelong M, Augagneur Y, Morzadec C, Jouneau S, et al. Crystalline Silica Impairs Efferocytosis Abilities of Human and Mouse Macrophages: Implication for Silica-Associated Systemic Sclerosis. Front Immunol. 18 févr 2020;11:219.

33. Ashcroft T, Simpson JM, Timbrell V. Simple method of estimating severity of pulmonary fibrosis on a numerical scale. Journal of Clinical Pathology. 1 avr 1988;41(4):467-70.

34. Zhang Y, Liang R, Chen CW, Mallano T, Dees C, Distler A, et al. JAK1-dependent transphosphorylation of JAK2 limits the antifibrotic effects of selective JAK2 inhibitors on long-term treatment. :9.

35. Yamamoto T, Nishioka K. Increased expression of p53 and p21 (Waf1/Cip1) in the lesional skin of bleomycin-induced scleroderma. Arch Dermatol Res. 1 mai 2005;296(11):509-13.

36. Wollin L, Trinh-Minh T, Zhang Y, Distler JHW. The effect of nintedanib versus mycophenolate mofetil in the Fra2 mouse model of systemic sclerosis-associated interstitial lung disease. Clin Exp Rheumatol. août 2021;39 Suppl 131(4):134-41.

37. Yamamoto T, Yokozeki H, Nishioka K. Fas- and FasL-deficient mice are resistant to the induction of bleomycin-induced scleroderma. Arch Dermatol Res. 1 févr 2007;298(9):465-8.

38. Skaug B, Khanna D, Swindell WR, Hinchcliff ME, Frech TM, Steen VD, et al. Global skin gene expression analysis of early diffuse cutaneous systemic sclerosis shows a prominent innate and adaptive inflammatory profile. Annals of the Rheumatic Diseases. 1 mars 2020;79(3):379-86.

39. Trombetta AC, Soldano S, Contini P, Tomatis V, Ruaro B, Paolino S, et al. A circulating cell population showing both M1 and M2 monocyte/macrophage surface markers characterizes systemic sclerosis patients with lung involvement. Respir Res. 2018;19:186.

40. Skaug B. Type I interferon dysregulation in Systemic Sclerosis. 2020;7.

41. Michlewska S, Dransfield I, Megson IL, Rossi AG. Macrophage phagocytosis of apoptotic neutrophils is critically regulated by the opposing actions of pro-inflammatory and anti-inflammatory agents: key role for TNF-α. The FASEB Journal. 2009;23(3):844-54.

42. York MR, Nagai T, Mangini AJ, Lemaire R, van Seventer JM, Lafyatis R. A macrophage marker, siglec-1, is increased on circulating monocytes in patients with systemic sclerosis

and induced by type i interferons and toll-like receptor agonists. Arthritis & Rheumatism. 2007;56(3):1010-20.

43. Herrmann M, Voll RE, Zoller OM, Hagenhofer M, Ponner BB, Kalden JR. Impaired phagocytosis of apoptotic cell material by monocyte-derived macrophages from patients with systemic lupus erythematosus. Arthritis & Rheumatism. 1998;41(7):1241-50.

44. Khanna D, Lin CJF, Furst DE, Wagner B, Zucchetto M, Raghu G, et al. Long-Term Safety and Efficacy of Tocilizumab in Early Systemic Sclerosis-Interstitial Lung Disease: Open-Label Extension of a Phase 3 Randomized Controlled Trial. Am J Respir Crit Care Med. 15 mars 2022;205(6):674-84.

45. Milara J, Hernandez G, Ballester B, Morell A, Roger I, Montero P, et al. The JAK2 pathway is activated in idiopathic pulmonary fibrosis. Respir Res. 6 févr 2018;19(1):24.

46. Distler O, Highland KB, Gahlemann M, Azuma A, Fischer A, Mayes MD, et al. Nintedanib for Systemic Sclerosis–Associated Interstitial Lung Disease. N Engl J Med. 27 juin 2019;380(26):2518-28.

47. Montero P, Milara J, Roger I, Cortijo J. Role of JAK/STAT in Interstitial Lung Diseases; Molecular and Cellular Mechanisms. Int J Mol Sci. 9 juin 2021;22(12):6211.

48. Wu M, Skaug B, Bi X, Mills T, Salazar G, Zhou X, et al. Interferon regulatory factor 7 (IRF7) represents a link between inflammation and fibrosis in the pathogenesis of systemic sclerosis. 2020;20.

49. Dees C, Tomcik M, Palumbo-Zerr K, Distler A, Beyer C, Lang V, et al. JAK-2 as a novel mediator of the profibrotic effects of transforming growth factor β in systemic sclerosis. Arthritis & Rheumatism. 2012;64(9):3006-15.

50. Valenzi E, Tabib T, Papazoglou A, Sembrat J, Trejo Bittar HE, Rojas M, et al. Disparate Interferon Signaling and Shared Aberrant Basaloid Cells in Single-Cell Profiling of Idiopathic Pulmonary Fibrosis and Systemic Sclerosis-Associated Interstitial Lung Disease. Front Immunol. 2021;12:595811.